THE ASTROPHYSICAL JOURNAL, 404:611–619, 1993 February 20

GINGA OBSERVATIONS OF THE COMA CLUSTER AND STUDIES OF THE SPATIAL DISTRIBUTION OF IRON

JOHN P. HUGHES
Harvard-Smithsonian Center for Astrophysics, 60 Garden Street, Cambridge, MA 02138

JACKIE A. BUTCHER AND GORDON C. STEWART
X-Ray Astronomy Group, Department of Physics, University of Leicester, University Road, Leicester, LE1 7RH, England, UK

AND

YASUO TANAKA
Institute of Space and Astronautical Science, 1-1, Yoshinodai, 3-chome, Sagamihara-shi, Kanagawa 229, Japan
Received 1991 February 25; accepted 1992 August 28

ABSTRACT

The large area counters on the Japanese satellite *Ginga* have been used to determine the X-ray spectrum from the central region of the Coma cluster of galaxies over the energy range from 1.5 to 20 keV. The spectrum is well represented by an isothermal model of temperature 8.21 ± 0.16 keV and a heavy element (iron) abundance of 0.212 ± 0.027, relative to the cosmic value. The *Ginga* spectrum was found to be consistent with the X-ray spectra from the *Tenma* and *EXOSAT* satellites for a large class of nonisothermal temperature distributions. The measured iron elemental abundances were used to set a lower limit on the total mass of iron in Coma under the assumption that the iron is not distributed uniformly throughout the cluster. The mass ratio of iron relative to hydrogen (within 2 Mpc) is not less than 18% of the cosmic iron to hydrogen mass ratio. This compares to an average abundance of 24% if the iron is distributed uniformly. We discuss these results in terms of models for the production of iron in galaxy clusters.

Subject headings: galaxies: clusters: individual (Coma) — galaxies: intergalactic medium — X-rays: galaxies

1. INTRODUCTION

The Coma cluster of galaxies has been observed by nearly all space-borne X-ray observatories. It is relatively nearby ($z = 0.0232$), extended (core radius $\sim 8'$), and luminous in X-rays ($\sim 10^{45}$ ergs s^{-1}) with a high gas temperature (~ 8 keV). As part of its performance verification program, the third Japanese X-ray astronomy satellite *Ginga* ("Galaxy") (Makino et al. 1987) observed the Coma cluster. In this article we report on the analysis and modeling of the *Ginga* X-ray spectral data.

The principal experiment on *Ginga* is the large area counter (LAC) (Turner et al. 1989), an array of eight sealed proportional counters with a total geometric collecting area of 4000 cm^2. The efficiency for absorbing X-rays is high (greater than 10%) from 1.5 to nearly 30 keV. These detectors have energy resolution of 18% (FWHM) at ~ 6 keV. The LAC has a very low internal background rate which makes it a very sensitive instrument for X-ray spectral studies. The field of view is mechanically collimated to 1°–2° (FWHM).

One of the aims of this research was to demonstrate consistency between the *Ginga* X-ray spectrum of the Coma cluster and the spectra obtained by the earlier *Tenma* (Hughes et al. 1988b) and *EXOSAT* (Hughes, Gorenstein, & Fabricant 1988a) satellites. These earlier studies showed that the Coma cluster almost certainly deviates from isothermality, and that a model with an isothermal core surrounded by a region with temperature decreasing radially outward could describe the spectral and imaging data. In addition, a large class of rather general models for the binding mass distribution of the Coma cluster was found to be consistent with the X-ray (as well as the optical galaxy and velocity dispersion) data (Hughes 1989). The present study confirms that these models describe the *Ginga* data, and rule out pure polytropic models of the form used to describe the *HEAO 1* A-2 observations of this cluster by Henriksen & Mushotzky (1986). For completeness, we have investigated the effects of background subtraction and detector gain uncertainties. We find that the uncertainty in most derived results (the metal abundance determination is an exception) is dominated by the inclusion of these systematic effects.

The spatial distribution of the metals in clusters of galaxies has been of interest for some time. At the most basic level, knowing the space distribution allows one to determine the total mass of iron in the cluster. Knowledge of the distribution also should yield clues to the source of the metal enrichment in clusters and perhaps to the origin and evolution of the hot gas itself. In this article we introduce a simple parameterization for the radial distribution of iron atoms in the cluster and use the observed metal abundances from four different spatial regions in the Coma cluster corresponding to the *Tenma*, *EXOSAT* (two separate data sets), and *Ginga* data sets to constrain the allowed iron distribution parameters. We find a strong lower limit to the mass of iron in the Coma cluster: the iron mass cannot be less than $\sim 75\%$ of the uniformly distributed value. We consider a simplified model for ram-pressure stripping of the enriched gas in Coma member galaxies by the intracluster medium. Our observations are not sensitive enough to be able to reject this scenario based solely on the predicted spatial distribution of iron.

This article is organized in the following manner. The next section (§ 2) discusses the *Ginga* data reduction, i.e., data selection criteria, background subtraction and gain determination. Next we describe our model fits in § 3 including nonisothermal temperature distributions and models for the spatial distribution of iron. Discussion and conclusions are in §§ 4 and 5.

2. DATA REDUCTION

Coma was observed by the large area counters (LAC) on *Ginga* on 1987 July 1 during the performance verification phase of the mission. There were 4352 s of data which satisfied several stringent data selection criteria (to be discussed below). The source yielded a total counting rate (top plus middle layers) of 162 s^{-1} (1.5–20 keV) and the spectrum was statistically well determined over this energy range. In each pulse height (PH) channel a systematic error of 1% of the source signal was added in quadrature with the statistical error to account for uncertainties in the energy bin boundaries. This value also was necessary to obtain an acceptable fit to the standard celestial X-ray calibration source (the Crab Nebula). In this work we explore separately systematic effects due to uncertainties in the gain of the LAC as well as the background subtraction. Further constraints on the systematic errors in the data and their analysis were obtained by comparison between results obtained using the independent analysis procedures available at Leicester and ISAS.

The gain of the LAC is monitored in flight using the Ag Kα line at 22.1 keV, which arises from fluorescence of cosmic X-ray background photons (plus cosmic-ray particles) in the silver coating on the LAC collimator. For this observation, we determined the Ag Kα line energy for each of the eight individual detectors in the top and middle layers. The raw count rate data in the energy range 16–30 keV was fitted with two power-law components to approximate the continuum and a doublet line (energy separation of 2.91 keV) was used to approximate the Ag Kα and Kβ line blends. The intensity of the Kβ line was fixed at a value equal to 0.1 of the Kα line intensity. This includes the difference in LAC detection efficiency at the energies corresponding to the two lines, as well as the intrinsic line ratio (Salem, Panossian, & Krause 1974). The LAC energy resolution function was included as $\Delta E/E = 0.18(E/5.9\ \mathrm{keV})^{-0.5}$.

The 16 individual gain values for the top and middle layers were combined (using an average based on weighting by the count rates in the two layers) to form eight gain values for the summed spectrum. An average response function computed from these gain values was used in the model fitting. Note that the overall average gain was such that the Ag Kα fluorescent line from the collimator fell in PH channel 35.25 ± 0.08 close to the nominal gain which lies between 35.0 and 35.2 (S. Takano, private communication). We use this value below to represent the systematic uncertainty in the LAC gain. Finally, the linearity of the LAC counters was determined prelaunch, and it was assumed that this remained stable during the mission.

The background of the LAC has been studied in great detail (Hayashida et al. 1989; Butcher et al. 1993). For background subtraction during the Coma observation, we used one of the techniques (so-called Method II) developed by these authors. We used four parameters: the SUD rate (counts above the upper discriminator level), the PIM rate (counts for LAC sense wires screened from the field of view), the charged particle cutoff rigidity (COR), and the argument of perigee of the satellite, to determine the intrinsic particle-induced background spectrum. (The large flux of this bright X-ray source gives a significant count rate in the MID rate often used as an additional background monitor.) For the diffuse extragalactic X-ray background, an average of a large number of source-free fields at high Galactic latitude was used.

This technique yielded excellent results. The 2–10 keV count rate of the cluster after background subtraction showed no time variability, and there were no residual correlations between this source count rate and the SUD rate, the PIM rate, or the COR. We also checked for correlations between the SUD rate and both the background-subtracted source count rate above PH channel 31 and the MID rate, which would be most sensitive to improper background subtraction. No significant correlations were found. Between $\sim$20 and 25 keV imperfect subtraction of the Ag Kα line introduced an S shaped artifact in the spectrum, but this can be attributed to the slightly higher fluorescence caused by the presence of Coma in the field of view. Hence we will only consider the spectrum out to 20 keV.

The principle uncertainty in the background subtraction arises from spatial fluctuations in the diffuse X-ray background (e.g., Warwick & Stewart 1989). From a large number of *Ginga* pointings toward apparently source-free regions of the sky these authors have determined the average spectrum of the diffuse background as viewed by *Ginga*. Furthermore they find that the rms deviation from pointing to pointing is $\sim$5% of the average spectrum. We use this rms spectrum to represent the systematic uncertainty in the background subtraction for this study of the Coma cluster.

Only data from the remote pass, which tends to have the lowest background on average, were used in this analysis. Earth's elevation angle was required to be larger than 20°. Data from regions in the satellite orbit corresponding to higher background (such as the SAA passage and orbital regions with COR < 10) were rejected. We rejected data from segments in which the LAC high voltage was turned on or off. Since the angle from the LAC field of view and the Sun was $\sim$83°, contamination from solar X-rays was possible. We restricted ourselves to data taken only in Earth's shadow and thereby discarded $\sim$9000 s of data. Since we intended to search for evidence of nonisothermality in the cluster X-ray spectrum, we required accurate knowledge of that spectrum even in the lowest energy channels (where solar scattered X-rays would have the largest effect). In addition, even for only 4352 s of data, the errors on the spectrum are dominated by the inclusion of a 1% systematic error (as discussed above), and the fitted parameters (temperature, iron abundance, etc.) are dominated by the systematic uncertainty in gain and background subtraction. We have summed the data from the top and middle layers as well as the eight individual detectors to form the spectrum, which we show in Figure 1. We carried out fits to each layer separately for the redshifted optically thin plasma emission model (see § 3.1.2 below) and the fitted results were consistent with each other at $\sim 1\ \sigma$. All quoted results are based on the summed spectrum in Figure 1. It should be noted, however, that the excluded data are entirely consistent with the restricted data set utilized here.

3. MODEL FITS

3.1. *Isothermal Temperature Distributions*

Isothermal models yield acceptable χ^2 values. We have considered two types of model fits: (1) bremsstrahlung continuum models with Kα and Kβ lines introduced as Gaussian profiles, and (2) redshifted optically thin collisional ionization equilibrium (CIE) thermal bremsstrahlung models (Raymond & Smith 1978; J. C. Raymond, private communication, hereafter RS). In both cases we fix the hydrogen column density to a

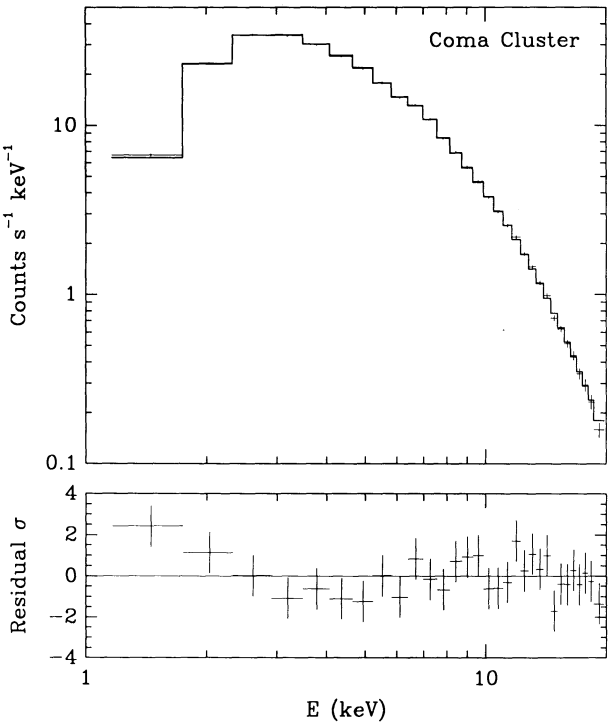

FIG. 1.—*Top panel: Ginga* X-ray spectrum of the Coma cluster with best-fit isothermal RS model. *Bottom panel:* Residual spectrum (observed data minus best-fit model).

value of $10^{20.3}$ cm^{-2}, which is well below the level to which the LAC is sensitive, is the average value determined from 21 cm measurements and is consistent with the value obtained from lower energy X-ray spectra (Gorenstein et al. 1979).

3.1.1. *Continuum plus Gaussian Lines*

The thermal bremsstrahlung model used for the continuum is based on the Gaunt factor for a pure hydrogen plasma (Karzas & Latter 1961) as calculated by Kellogg, Baldwin, & Koch (1975). In order to simulate a narrow line, the energy width of the Gaussian lines was fixed at 0.1 keV, significantly less than the energy resolution of the LAC at ~7 keV. The introduction of both Kα and Kβ lines was highly significant: the minimum χ^2 values were 229.2, 32.6, and 20.8 for fits with no, one, and two lines. The results of this fit are summarized in Table 1. We have also used another calculation of the Gaunt factor (Gould 1980, 1981) and the best-fit temperature in this case was 7.96 ± 0.09 with a χ^2 value of 19.5. The energies and equivalent widths of the emission lines were virtually unchanged from the ones shown in Table 1.

The redshifted Fe lines lie at energies of 6.79 ± 0.09 keV and 8.50 ± 0.40 keV and the redshifted temperature is 8.26 keV. We have determined the expected values for the line energies and ratio of Kα to Kβ line emission to be 6.772, 8.163, and 5.97 (at the redshifted temperature) from the calculations of RS. The agreement is excellent. The calculated equivalent width assuming cosmic abundances (Fe/H ratio of 4×10^{-5} by number) is 972 (252) eV for Kα (Kβ), requiring an abundance of 0.225 (0.250) for the Coma cluster.

For comparison to the *Tenma* results (Okumura et al. 1989) we have fitted our data with the Gaunt factor based on the calculations of Matteson (1971) and Maxon & Corman (1967) which these authors used. While this model yielded a χ^2 value of 70.4 for the *Ginga* data, which allows us to reject it at greater than 99.95% confidence, there was good agreement for the fitted Fe line energies and equivalent widths, although the emission integral and best-fit temperatures were different. This difference between data sets is also apparent when the RS model is used (see below) and is a result of the differing fields of view of the two instruments and represents strong evidence for a nonisothermal temperature distribution in the Coma cluster.

TABLE 1

BEST-FIT PARAMETERS: CONTINUUM PLUS GAUSSIAN LINES

Parameter	Best-Fit value[a]
Emission integral (n^2V)[b] (10^{67} cm^{-3})	9.81 ± 0.11
Continuum temperature (keV)	8.07 ± 0.09
Kα line equivalent width (eV)	219 ± 30
Kα line energy (keV)	6.64 ± 0.09
Kβ line equivalent width (eV)	63 ± 31
Kβ line energy (keV)	8.31 ± 0.42
Kα to Kβ ratio	5.81 ± 2.91
n_H (atoms cm^{-2})	2×10^{20}
χ^2 (d.o.f)	20.8 (25)

[a] Statistical errors at 90% confidence for one interesting parameter.
[b] Uses geometric collecting area of 4000 cm^2, average transmission of 0.70, and $H = 50$ km s^{-1} Mpc^{-1}.

3.1.2. *RS Thermal Models*

The best-fit values for the parameters of this model are shown in Table 2 and the best-fit spectrum is plotted in Figure 1. The photon spectrum, based on the best-fit parameters for this model, is shown in Figure 2. The iron abundance is consistent with the value derived above from the fits to a continuum model with Gaussian lines. For the RS model the abundances of C, N, O, Ne, Mg, Si, S, Ar, Ca, Fe, and Ni were varied both in unison and with the Fe abundance separate, while the He/H ratio was fixed at 0.085. Previous analyses of data from *Tenma* and *EXOSAT* have used the same model (Hughes et al. 1988a, b) and thus a comparison of the results on temperature can be made easily and reliably (see Table 3). Each of the four sets of data in Table 3 yielded acceptable fits for isothermal models, yet each of the temperatures measured was different! However, the pattern is clear: the larger the field of view, the lower the measured temperature. In column (4) of Table 3 we give the average effective radius (the radius weighted by the cluster surface brightness and collimator response) of each observation.

TABLE 2

BEST-FIT PARAMETERS: RS MODEL

Parameter	Best-Fit Value[a]
Emission integral ($n_H^2 V$)[b] (10^{67} cm^{-3})	9.37 ± 0.09
Continuum temperature (keV)[c]	8.21 ± 0.09[d]
Abundance[e,f]	0.212 ± 0.026[g]
n_H (atoms cm^{-2})	2×10^{20}
χ^2 (d.o.f)	27.5 (28)

[a] Statistical errors at 90% confidence for one interesting parameter.
[b] Uses geometric collecting area of 4000 cm^2, average transmission of 0.70, and $H = 50$ km s^{-1} Mpc^{-1}.
[c] Source temperature ($z = 0.0232$).
[d] Statistical error only. Error including systematics is ±0.16 keV.
[e] Relative to cosmic: [Fe]/[H] = 4×10^{-5}.
[f] With iron tied to other heavy elements; with iron free $A_{Fe} = 0.19$.
[g] Statistical error only. Error including systematics is ±0.027.

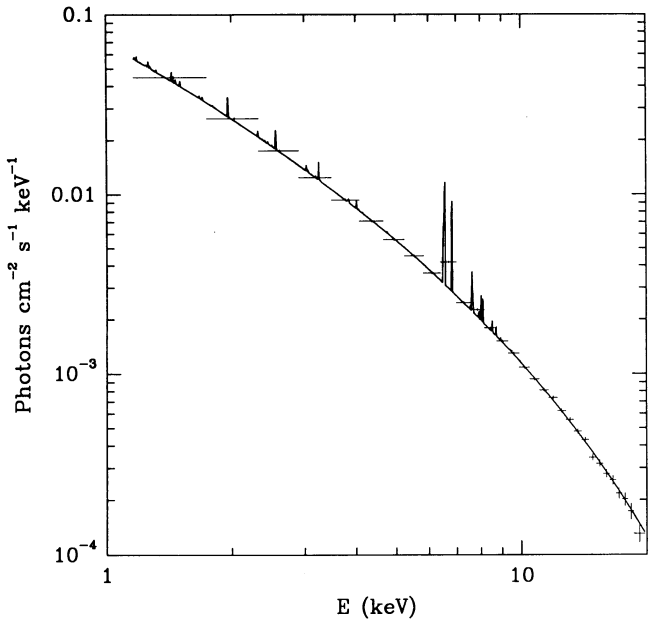

FIG. 2.—Incident photon spectrum of the Coma cluster from the best-fit isothermal RS mode'.

Before investigating nonisothermal temperature distributions, we would like to examine the dependence of some of our present *Ginga* results on the uncertainty in gain and background subtraction. We generated results for plus and minus 1 σ variation in gain and background subtraction, using the values determined in § 2. The best-fit temperature changed by ± 0.13 keV when the gain was varied and by ± 0.04 keV when the background was varied. These in fact dominate the statistical error on the temperature determination. If we add the systematic and statistical errors in quadrature, we derive a total error on the temperature of ± 0.16 keV. The iron abundance was much less sensitive to these variations, changing by only ± 0.005 (gain) and ± 0.002 (background). If we again add systematic and statistical errors in quadrature, the total uncertainty in abundance becomes ± 0.027. We show this graphically in Figure 3. We plot contours of constant χ^2 at the 90% confidence level for temperature (kT) versus iron abundance ($\chi^2_{\rm min} + 4.61$; Avni 1976; Lampton, Margon, & Bowyer 1976) for five data sets: (1) nominal gain, nominal background subtraction; (2) higher gain, more background; (3) lower gain, more background; (4) higher gain, less background; and (5) lower gain, less background. It is clear that the dominant uncertainty arises from systematic errors in the gain and background subtraction.

Before leaving this section, we wish to describe our limits on nonthermal (i.e., power law) emission from the Coma cluster.

TABLE 3

TEMPERATURE MEASUREMENTS OF THE COMA CLUSTER

Instrument	kT (keV)	FOV	$R_{\rm eff}$	Reference
Tenma	7.5 ± 0.2	3°	20′	1
EXOSAT	8.50 ± 0.3	0.75	11	2
EXOSAT	7.39 ± 0.7	0.75	22	2
Ginga	8.21 ± 0.2	1 × 2	14	3

REFERENCES.—(1) Hughes et al. 1988b; (2) Hughes et al. 1988a; and (3) this work.

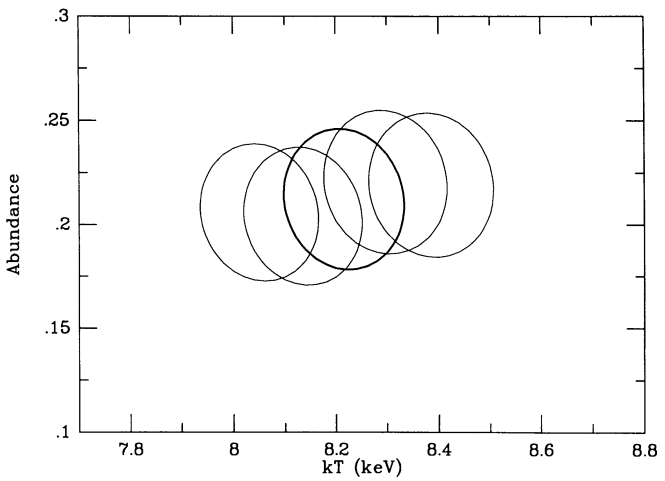

FIG. 3.—Results of fits to the *Ginga* X-ray spectrum of Coma. Two-dimensional χ^2 contours at the 90% confidence level for fractional iron abundance vs. temperature using the isothermal RS model. The five curves correspond to the five data sets with systematic variations in the background subtraction and detector gain. The bold curve corresponds to nominal gain and background subtraction.

We find no significant evidence for a high-energy tail in the X-ray spectrum out to almost 40 keV. Our data allows us to set limits to the on-axis power-law emission (flux at 1 keV) of 1.6×10^{-3} photons cm^{-2} s^{-1} keV^{-1} for a photon index of 1.33, 7.7×10^{-3} photons cm^{-2} s^{-1} keV^{-1} for an index of 1.77, and 1.8×10^{-2} photons cm^{-2} s^{-1} keV^{-1} for an index of 2.21. These values are about an order of magnitude less than values quoted by balloon-borne hard X-ray experiments: Bazzano et al. (1984) and more recently by Fusco-Femiano et al. (1993) and are insensitive to the assumed absorption for the power-law component.

3.2. *Nonisothermal Temperature Distributions*

3.2.1. *Ginga Collimator Response*

Accurate knowledge of the collimator response is essential for the study of nonisothermal temperature distributions in large diffuse clusters such as Coma. Fortunately, the *Ginga* collimator has been well-studied thanks to the analysis of observations of SN 1987a in the Large Magellanic Cloud (Dotani et al. 1987). From scans of the Crab Nebula the energy dependence of the collimator has been calibrated in flight. Lower energy X-ray photons have a broader response than higher energy ones, due to scattering from the collimator. We constructed a collimator response including this scattered component using the observed spectrum of Coma. The top panel of Figure 4 shows the average *Ginga* transmission as a function of radial distance from the center of the Coma cluster ($\alpha_{1950} = 12^{\rm h}57^{\rm m}19^{\rm s}$, $\delta_{1950} = 28°13'7''$; Abramopoulos, Chanan, & Ku 1981). The full width at half-maximum of this response curve is $\sim 80'$. The lower panel shows the average transmission times the area at each radius (the curve which is higher beyond $\sim 20'$) and the product of that curve with the X-ray surface brightness of Coma from Hughes et al. (1988b). The latter curve peaks at $\sim 10'$ in the figure. The vertical dashed line at 14.2 is the average effective radius of this observation.

We compared this response to a purely geometric model of the collimator (i.e., one with no scattered component). Differences between the two only became apparent beyond

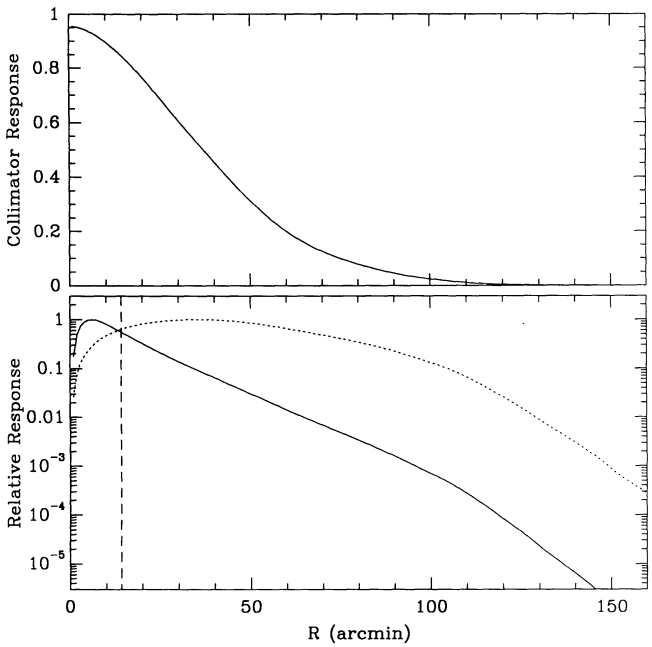

FIG. 4.—*Top panel:* Average *Ginga* collimator transmission as a function of radial distance from the center of the Coma cluster. *Bottom panel:* Average transmission times the area at each radius (*dotted curve*) and the product of that curve with the X-ray surface brightness of Coma (*solid curve*). The vertical dashed line at 14'.2 is the average effective radius of this observation.

~70', where the average response is less than 10% and the surface-brightness–weighted response is more than two orders of magnitude less than near the center. We also constructed collimator responses for slightly different pointing positions relative to the center of the Coma cluster. From among the subframes of accepted data, we chose the two pointing positions with the highest and lowest transmission at the cluster center. The response functions constructed from these were different by less than 1% over the whole radial range sampled. Finally, we used each of these collimator response functions for our analysis of nonisothermal temperature distributions (see immediately below) and the fitted parameters were indistinguishable.

3.2.2. *Isothermal/Polytropic Hybrid Models*

In previous work (Hughes et al. 1988a, b) a model for the nonisothermal temperature distribution of the Coma cluster was introduced, which successfully described the *Tenma* and *EXOSAT* X-ray spectra of the cluster. We use this same model for the *Ginga* data. Briefly, we assume that the temperature of the cluster is isothermal (at value T_{ISO}) out to a certain radius (R_{ISO}), beyond which the temperature decreases as a polytrope (density and temperature related through the equation $T \propto \rho^{\gamma-1}$). The radius and temperature of the isothermal region are variables to be determined by fitting to the data, while the polytropic index of the outer region ($\gamma = 1.555$) and the parameters describing the X-ray surface brightness ($R_{core} = 6'.9$ and $\beta = 0.60$) are fixed at the values used in the previous analyses. For each trial value of T_{ISO} and R_{ISO} a model spectrum based on the RS plasma emission model (appropriately redshifted) is generated in the following manner. We divide the cluster into a large number of constant temperature radial shells. Each shell is projected onto the plane of the sky, weighted by the square of its hydrogen number density, and convolved with the *Ginga* collimator response. This gives the weighting factor for this temperature value. An isothermal RS model is calculated at each temperature and multiplied by the weighting factor. The final spectrum is the sum of these individual spectra from the various radial shells.

For the data set with nominal gain and background subtraction, we find that this model yields a slightly better χ^2 value than the isothermal model (25.1 vs. 27.5 for 27 and 28 d.o.f., respectively), although the reduction in χ^2 is not significant. The best-fit values, $T_{ISO} = 8.8$ keV and $R_{ISO} = 4.2$ (in units of R_{core}), are consistent with the *EXOSAT* results at 68% confidence and with the *Tenma* results at better than 90% confidence. In addition, the 68% confidence contours for all three data sets have a significant region of overlap in parameter space around $T_{ISO} = 9$ keV and $R_{ISO} = 3.5$.

The systematic uncertainty in gain and background subtraction have a large effect in this study. We show this in Figure 5 for the five *Ginga* data sets representing these systematic uncertainties. We show contours of constant χ^2 at 90% confidence in the T_{ISO}, R_{ISO} parameter space. The cross shows the best-fit result with 90% errors from the combined *Tenma* and *EXOSAT* analysis. Even when the systematics are included, the *Ginga* data are slightly more constraining for this model than the *EXOSAT* data alone. This is due to the higher statistical signal of the *Ginga* data, as well as the lower background and higher energy response of *Ginga*. However, because of the large angular size of the *Ginga* collimator, it is not likely that one will be able to obtain high-quality spectra from a set of spatially disjoint regions of the cluster as was done with *EXOSAT* by Hughes et al. (1988a).

We have reproduced the outer envelope of the contours shown in Figure 5 by fitting to the nominal *Ginga* data set with the inclusion of additional systematic error. After some trial and error, we found that a total systematic error of 4%–5% roughly reproduces the envelope of contours.

For completeness we have also fit the *Ginga* data with the polytropic models used by Henriksen & Mushotzky (1986). For $\beta = 0.6$, we find a best-fit value of the central temperature $T_e = 9.0^{+2.8}_{-0.9}$ keV and polytropic index $\gamma = 1.05^{+0.11}_{-0.05}$ but this

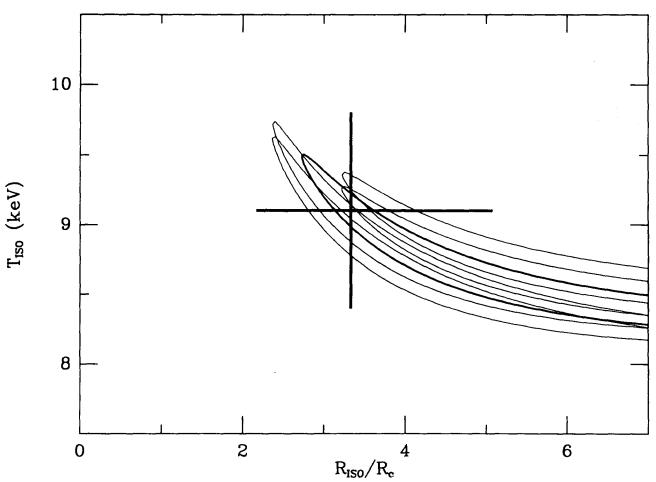

FIG. 5.—Results of fits to a nonisothermal temperature model, consisting of an isothermal core surrounded by a polytropic distribution. We display two-dimensional χ^2 contours at the 90% confidence level for the temperature of the isothermal region (T_{iso}) vs. its radius (R_{iso}) in units of the core radius. The five curves correspond to the five data sets with systematic variations in the background subtraction and detector gain. The bold curve corresponds to nominal gain and background subtraction. The cross designates the allowed region of parameter space from the combined analysis of *Tenma* and *EXOSAT* X-ray spectra.

model is not a significant improvement on the isothermal model. Fixing β at a value of 0.76 as used by Henriksen & Mushotzky results in values of $T_c = 8.45^{+2.4}_{-0.4}$ keV and $\gamma = 1.015^{+0.12}_{-0.015}$, significantly different from the revised allowed range of γ determined by Cowie, Henriksen, & Mushotzky (1987) of $1.33 < \gamma < 1.43$.

Figure 5 demonstrates rather clearly the problem with interpreting global integrated X-ray spectral data for clusters of galaxies in terms of nonisothermal models. It is obvious that variations in gain and background subtraction can mimic the effects under investigation. Only truly spatially distinct spectral observations (as done crudely in the *EXOSAT* study and which will become routine with the X-ray facilities planned for later this decade) can give reliable results about the distribution of temperatures in clusters of galaxies. However, at this juncture, based on data from three different experiments the evidence is compelling that the gas in the Coma cluster consists of material emitting over a large range of temperatures.

3.3. *Spatial Distribution of Iron*

The results of isothermal fits to the *Ginga*, *Tenma*, and *EXOSAT* spectra all yield rather similar values for the fractional iron abundance ($\sim$20%). In this section we discuss the constraints that can be applied to the spatial distribution of iron in the Coma cluster from these observations. Immediately below we describe the reanalysis of the *Tenma* and *EXOSAT* data using nonisothermal models to obtain a self-consistent set of iron abundance values. Then we describe our parameterization for the spatial distribution of iron in the cluster and how we use the measured abundances as constraints.

3.3.1. *Analysis*

The present iron abundance values from the different instruments are based on fits to (different) isothermal temperature models, i.e., the temperatures presented in Table 3. In general, fitted values for the iron abundance are sensitive to the continuum temperature due to both the intrinsic variation of iron line flux with temperature and the change in continuum shape near the line. In the case of Coma, we have already argued that the global X-ray spectrum is best described by a nonisothermal model with a radial temperature gradient. For these reasons, we have refitted the *Tenma* and *EXOSAT* spectra using the best-fit nonisothermal temperature model discussed above to derive self-consistent iron abundance values from the different instruments. As in the *Ginga* analysis discussed above, the model was projected onto the plane of the sky and convolved with the collimator response appropriate to the instrument under study.

X-ray fluxes and fractional iron abundances derived from fits to the best-fitting nonisothermal model (with parameters $T_{\rm ISO} = 9.1$ keV and $R_{\rm ISO} = 3.33\,R_{\rm core}$) are shown in Table 4. The measured flux values clearly depend on the field-of-view of the instrument (increasing from *EXOSAT* to *Ginga* to *Tenma*), while the iron abundance is consistent with a uniform value of 0.239 ± 0.013. This set of measured iron abundances can be used to derive a strong lower limit on the amount of iron present in the cluster.

3.3.2. *Models for the Iron Distribution*

We have chosen a convenient well-known three-parameter form for the distribution of iron atoms as a function of radius in the cluster

$$n_{\rm Fe} = n_{\rm Fe,0}[1 + (R/R_{\rm Fe})^2]^{-3\beta_{\rm Fe}/2} ,$$

TABLE 4

X-RAY FLUXES AND IRON-ABUNDANCE MEASUREMENTS OF THE COMA CLUSTER FOR BEST-FIT HYBRID MODEL[a]

Instrument	2–10 keV Flux (ergs cm^{-2} s^{-1})	Iron Abundance
Tenma	3.66×10^{-10}	0.237 ± 0.017
EXOSAT (center)	2.84×10^{-10}	0.231 ± 0.032
EXOSAT (off-center)	0.39×10^{-10} [b]	$0.344^{+0.081}_{-0.146}$
Ginga	3.39×10^{-10}	0.247 ± 0.024

[a] $T_{\rm ISO} = 9.1$ keV, $R_{\rm ISO} = 3.33$.
[b] Average of three pointings: east, west, and south of cluster center.

and our program entails determining what values of $n_{\rm Fe,0}$ $R_{\rm Fe}$, and $\beta_{\rm Fe}$ are allowed by the abundance values in Table 4. The distribution of hydrogen atoms is given by the same functional form but with values for $R_{\rm H}$ and $\beta_{\rm H}$ set by the X-ray surface brightness distribution (from the *Einstein* IPC image). This simplification requires that the 0.5–4 keV X-ray surface brightness be dominated by emission from hydrogen and helium atoms, i.e., that the iron enrichment be nowhere very extreme. We have confirmed post facto that this requirement is satisfied for the range of models we accept.

First we determined the projected surface brightness emission from iron

$$\Sigma_{\rm Fe}(R) = 2\int_R^\infty \frac{dr\,r}{\sqrt{r^2 - R^2}}\, n_{\rm Fe}(r) n_{\rm H}(r) \Lambda_{\rm Fe}[T(r)] .$$

Here we show the implicit dependence of the iron Kα line emissivity function $\Lambda_{\rm Fe}$ (calculated using the RS model) on the temperature distribution. Next we convolved both the iron surface brightness distribution and the overall X-ray surface brightness with the various collimator response functions and took the ratio of these values. Comparison with the iron abundance data results yielded the overall normalization of the model iron distribution and a χ^2 value for the given set of $R_{\rm Fe}$ and $\beta_{\rm Fe}$ values. For a given value of $R_{\rm Fe}$, $\beta_{\rm Fe}$ was reasonably well constrained by the data: for example with $R_{\rm Fe} = 10'$, we found $\beta_{\rm Fe} = 0.52^{+0.32}_{-0.19}$ (90% confidence level). However we were considerably less sensitive to variations in $R_{\rm Fe}$; values from 0.01 to 100′ all yielded essentially similar quality fits (for different $\beta_{\rm Fe}$ values of course).

Nevertheless, when the allowed range of $R_{\rm Fe}$ and $\beta_{\rm Fe}$ values is used to determine the total mass of iron contained within a given radius of the cluster center, the data are quite constraining. In Figure 6 we show the total mass of iron relative to hydrogen (relative to the cosmic mass ratio) contained within a 2 Mpc radius (at 90% confidence). The minimum mass of iron (19% of the cosmic value) is obtained for $R_{\rm Fe}$ values of 0.1 or less. Note that within a radius of 3 Mpc (nearly 10 optical or X-ray core radii) the minimum iron mass decreases to only 17%. Recall that the mass of iron is 24% under the uniform abundance distribution, which corresponds to an iron mass of $1 \times 10^{11}\,M_\odot$ (within 2 Mpc). In the next section we discuss the implications of these constraints on scenarios for the elemental enrichment of the intracluster medium.

4. DISCUSSION

4.1. *Cluster Binding Mass Determination*

It is well known that one of the important uses of X-ray spectral data is the determination of cluster binding masses. In

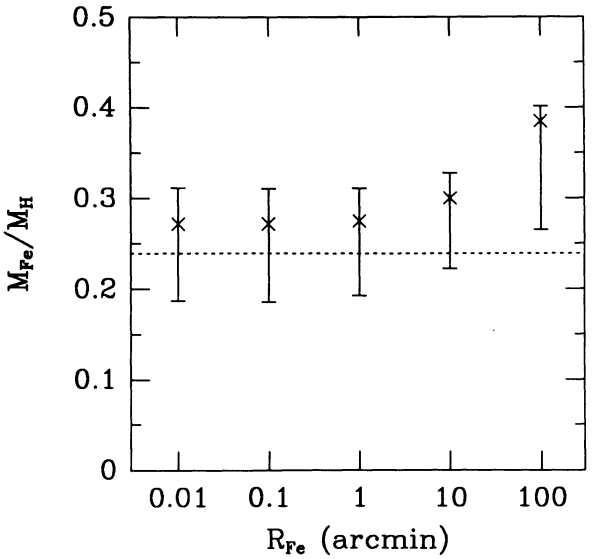

FIG. 6.—Ratio of total mass (within 2 Mpc) of iron relative to hydrogen (relative to the cosmic value of 4.0×10^{-5}) vs. the core radius for the spatial distribution of iron atoms. For each iron core radius plotted, the range in mass ratios comes from the allowed range in β_{Fe} at 90% confidence. The mass ratio corresponding to the best-fit β_{Fe} at each iron core radius is plotted as a cross. The uniform iron abundance value of 0.238 is shown as the dotted line.

an earlier study of the Coma cluster (Hughes 1989), *Tenma* and *EXOSAT* spectral data were used with *Einstein Observatory* imaging data to determine the allowed binding mass distributions. We have chosen the preferred mass distribution model from that article, i.e., where the binding mass follows the distribution of optical light, calculated the X-ray spectrum from the model temperature distribution and fitted to the *Ginga* Coma spectrum. The inferred mass of the cluster as determined by the best fit to the *Ginga* spectrum is entirely consistent with the value obtained in the previous study. The value obtained by *Ginga* for the central binding mass density ρ_{b0} is $1.02^{+0.05}_{-0.04} \times 10^{-25}$ g cm^{-3} (68% confidence level for one interesting parameter). However, including effects of background subtraction and gain uncertainty on the *Ginga* spectral data greatly increases the range of allowed central ρ_{b0} values. In fact, since it is not possible to determine the radial gradient of the temperature distribution from only the integrated X-ray spectrum, it is not possible even to determine the minimum allowed binding mass of the cluster from the *Ginga* data alone. Improvement in determining the binding mass of the Coma cluster may be possible with existing *Ginga* scanning data (H. Kondo, private communication) and significant improvements will be possible with Astro-D and Spectrum X-γ. Watt et al. (1991) recently used data on the center of the Coma cluster from Spacelab 2 to constrain the temperature distribution and thereby the virial mass distribution. Their results are consistent with those presented here.

4.2. *Iron Spatial Distribution*

If the iron in galaxy clusters is primordial, from a very early generation of stars or if all of the gas in the cluster was lost by the member galaxies, then the present distribution of iron should be nearly the same as the gas, if the settling time scale is as large as believed (Rephaeli 1978). This is certainly allowed by the observational constraints, and in fact it corresponds very nearly to the best-fit case with $\chi^2 = 1.3$ for 3 d.o.f. (confidence level for rejection is 26.7%). If the iron in galaxy clusters is a result of gas processed by stars in the member galaxies which was lost to the intracluster medium *irrespective* of the galaxy's position or velocity, then the spatial distribution of iron should be roughly proportional to the galaxy space density. This too is allowed, although it is a poorer fit to the data yielding $\chi^2 = 5.5$ again for 3 d.o.f. (confidence level for rejection is 86.3%).

Let us consider next a stripping scenario, wherein most of the hydrogen is primordial, but the iron is a result of ram-pressure stripping of the gas in the member galaxies by the intracluster medium. In this case the iron distribution should be proportional to $n_{gal} S_E$, where n_{gal} is the source term for the iron and S_E is the stripping efficiency. The latter quantity varies from 0 to 1 and represents the fraction of total available gas in the galaxy which is removed by ablation. That is to say, when the efficiency for stripping is high, as it is near the core of the cluster, then this quantity would be near unity, while in the outskirts of the cluster where stripping is less efficient, the value would be closer to zero.

In order to pursue a more quantitative discussion we have employed the results of Gaetz, Salpeter, & Shaviv (1987, hereafter GSS), who studied the effects of steady state ram pressure ablation from spherical galaxies using a hydrodynamical simulation. GSS introduce a quantity called Φ, which is the total mass fraction retained by the galaxy; we clearly want $S_E = 1 - \Phi$. With the relations in GSS we obtain

$$S_E = 1 - [1 + (\xi/0.6)^{1.23}]^{-1} ,$$

where

$$\xi = 91 f_{GSS} \left(\frac{v}{1750 \text{ km s}^{-1}} \right)^{2.4} \left(\frac{n_{gas}}{10^{-3} \text{ cm}^{-3}} \right) .$$

We have set model parameter values to those corresponding to GSS's standard galaxy, which has a luminosity of $2 \times 10^{10} L_\odot$ and a mass-to-light ratio of 20 (in solar units). These are reasonable values for bright galaxies in Coma. The other relevant model parameters are the internal galaxian gas replenishment rate, assumed to be 0.6 $M_\odot$ yr^{-1}, and the radial extent of the gas replenishment distribution. As formulated by GSS, the latter quantity can be expressed equivalently in terms of the effective half-mass radius for the gravitational mass distribution; GSS assume a value of 17.4 kpc. This value, in particular, is rather uncertain and so we include a fudge factor f_{GSS} to account for this, plus other, uncertainties in the galaxy model. We assume a constant value (independent of radial position) for the galaxy speed, and use the measured velocity dispersion of Coma (1010 km s^{-1}; Zabludoff, Huchra, & Geller 1990), converted to a three-dimensional value of 1750 km s^{-1}.

For $f_{GSS} = 1$, we find almost no difference in the expected iron distribution compared to the case where the iron is distributed like the galaxies. Quantitatively we obtain $\chi^2 = 5.7$ for 3 d.o.f. (confidence level for rejection is 87.2%). This can be understood by realizing that stripping is extremely efficient in this situation and that S_E is close to unity over most of the cluster. In fact S_E drops to a value of 0.5 only at the considerable distance of 7.3 Mpc from the cluster center. For a case with f_{GSS} lowered to 0.1 (corresponding roughly to decreasing the galaxy half-mass radius by a factor of 3), the iron distribution deviates somewhat more from the galaxy distribution. A fit to the data yields a χ^2 of 7.0 for 3 d.o.f. corresponding to a confidence level for rejection of 92.7%. Here the half-value

radius for S_E is 2.1 Mpc, where the gas density is 6.6×10^{-5} cm^{-3}.

There is some observational evidence that ram-pressure stripping has been efficient in the core of the Coma cluster. Observations of Coma cluster member galaxies in H I (Bothun, Schommer, & Sullivan 1984) and Hα (Kennicutt, Bothun, & Schommer 1984) reveal a significant deficit of both types of emission for the galaxies located within $\sim 1°$ (~ 2.4 Mpc) of the center. This suggests that it would not be realistic to lower f_{GSS} to values much below 0.1. Unfortunately, then, given the results in the preceding paragraph, we are not able to constrain strongly the amount of iron in the Coma cluster which could have been stripped out of the galaxies, based solely on the current data for the spatial distribution of iron. Other authors (Arnaud et al. 1992), however, have considered the origin of the total *amount* of iron seen in galaxy clusters and have concluded that it is probably impossible to produce using a standard iron yield from the current galaxy population. With new sensitive data on the spatial distribution of iron in clusters of galaxies expected from upcoming X-ray astronomy missions, we will be able to confirm these conclusions.

Our result on the iron distribution for Coma seems to be at odds with the results from the Spacelab 2 coded mask observations of Perseus (Ponman et al. 1990), who find a strong gradient in the iron abundance of the intracluster medium and thus derive a total iron mass which is about a factor of 4 less than the homogeneous value. First we note that a simple reanalysis of the outermost four abundance data points shown in Figure 2*a* of Ponman et al. suggests a uniform abundance component in Perseus of $0.15^{+0.23}_{-0.15}$ (relative to the cosmic value used here), which is not so different from the uniform value for Coma. The difference between the clusters lies in the presence of an abundance gradient in the core of the Perseus cluster, which contains an active galaxy and a strong cooling flow and therefore is a considerably more complicated system to model than Coma. Furthermore, preliminary analysis of BBXRT data for Perseus (Mushotzky 1991) does not support the claims of Ponman et al. regarding the iron distribution. Lastly, the analysis we present here for the gas stripping model shows that it is extremely difficult to produce strong gradients in the iron distribution in the cores of rich clusters. Clearly it will be interesting to follow up both results on Coma and Perseus with new observations, and to study the spatial distribution of iron in a large sample of additional clusters.

5. CONCLUSIONS

The X-ray spectrum of the Coma cluster of galaxies has been measured by the LAC onboard the *Ginga* satellite. The spectrum was statistically well determined from 1.5 to 20 keV. From this data, we have measured the gas temperature of the Coma cluster and find that it can be represented by an isothermal model of temperature 8.21 ± 0.16 keV with an iron abundance relative to the cosmic value (Fe/H $= 4.0 \times 10^{-5}$) of 0.212 ± 0.027. The dominant source of uncertainty in the fitted results arise from systematic uncertainties in the gain and background subtraction.

We have shown that the *Ginga* X-ray spectrum of the Coma cluster is entirely consistent with results from *Tenma* and *EXOSAT*. Although each data set yielded a different isothermal temperature, the several observed temperatures are quantitatively consistent with each other and arise from the different regions of the cluster observed by the different instruments. The temperature must decrease with radius from the center of the cluster, since the instruments with larger fields of view (*Tenma*) show lower temperatures than those with smaller ones (*EXOSAT* and *Ginga*). Detailed fits to a particular nonisothermal model yield consistent results at better than 68% confidence among the data sets.

The *Ginga* spectrum was also used to determine the binding mass of the cluster under the assumption that the binding mass is distributed as the galaxies, using the techniques developed by Hughes (1989). Again, the *Ginga* results were found to be consistent with those from *Tenma* and *EXOSAT*. Because of the uncertainty in gain and background subtraction, the *Ginga* data alone were not able to constrain significantly the allowed binding mass values.

We have set limits on the spatial variation of iron in the Coma cluster. The observed iron abundance values from the various data sets were used to set a strong lower limit on the total mass of iron contained in the cluster: within 2 Mpc the mass of iron relative to hydrogen is not less than 18% of the cosmic value. Under the assumption that the iron is distributed uniformly in space, then the average abundance is about 24%. We examined various scenarios for the origin of the iron in the Coma cluster and found that abundance distributions which are proportional to either the gas space density or the galaxy space density are fully consistent with the observational data. A simplified model for ram-pressure stripping of the gas in member galaxies was considered and the resulting abundance distributions were also found to be reasonably consistent with the current observations. One interesting result of this modeling attempt was the fact that a strong gradient in the abundance distribution did not arise from the ram-pressure stripping model. Data from future X-ray astronomy satellites will allow us to discriminate between these various scenarios for the origin of the heavy elements in galaxy clusters.

Thanks are extended to the large number of scientists, engineers, and technicians who conceived, designed, built, launched and operated *Ginga*. We also would like to thank the team that designed and built the LAC. We appreciate K. Hayashida's and O. R. Williams's significant contribution to modeling of the LAC background. We acknowledge useful discussions with M. Arnaud, W. Forman, P. Gorenstein, and C. Jones. We also appreciate the referee's helpful comments concerning our ram-pressure stripping model for the iron distribution. J. P. H. was supported under NASA grants NAG8-699 and NAG8-181. G. C. S. acknowledges receipt of an SERC advanced fellowship and J. A. B. an SERC research studentship.

REFERENCES

Aranaud, M., Rothenflug, R., Boulade, O., Vigroux, L., & Vangioni-Flam, E. 1992, A&A, 254, 49
Abramopoulos, F., Chanan, G. A., & Ku, W. H.-M. 1981, ApJ, 248, 429
Avni, Y. 1976, ApJ, 210, 642
Bazzano, A., Fusco-Femiano, R., La Padula, C., Polcaro, V. F., Ubertini, P., & Manchanda, R. K. 1984, ApJ, 279, 515
Bothun, G. D., Schommer, R. A., & Sullivan, W. T., III. 1984, AJ, 89, 466
Butcher, J. A., et al. 1993, in preparation
Cowie, L. L., Henriksen, M., & Mushotzky, R. 1987, ApJ, 317, 593
Dotani, T., et al. 1987, Nature, 330, 130
Fusco-Femiano, R., Bazzano, A., Ubertini, P., Perotti, F., Quadrini, E., & Dean, A. J. 1993, in Proc. Workshop on Supercluster and Clusters of Galaxies and Environmental Effects, in press
Gaetz, T. J., Salpeter, E. E., & Shaviv, G. 1987, ApJ, 316, 530 (GSS)

Gorenstein, P., Fabricant, D., Topka, K., & Harnden, F. R., Jr. 1979, ApJ, 230, 26
Gould, R. J. 1980, ApJ, 238, 1026; Erratum, 243, 677 (1981)
Hayashida, K., et al. 1989, PASJ, 41, 373
Henriksen, M. J., & Mushotzky, R. F. 1986, ApJ, 302, 287
Hughes, J. P. 1989, ApJ, 337, 21
Hughes, J. P., Gorenstein, P., & Fabricant, D. 1988a, ApJ, 329, 82
Hughes, J. P., Yamashita, K., Okumura, Y., Tsunemi, H., & Matsuoka, M. 1988b, ApJ, 327, 615
Karzas, W., & Latter, R. 1961, ApJS, 6, 167
Kellogg, E., Baldwin, J. R., & Koch, D. 1975, ApJ, 199, 299
Kennicutt, R. C., Bothun, G. D., & Schommer, R. A. 1984, AJ, 89, 1279
Lampton, M., Margon, B., & Bowyer, S. 1976, ApJ, 208, 177
Makino, F., & Astro-C Team. 1987, Astrophys. Lett. Comm., 25, 223
Matteson, J. L. 1971, Ph.D. thesis, University of California, San Diego
Maxon, M. S., & Corman, E. G. 1967, Phys. Rev., 163, 156
Mushotzky, R. 1991, in Proc. NATO ASI on Clusters and Superclusters of Galaxies, 91
Okumura, Y., Tsunemi, H., Yamashita, K., Matsuoka, M., Hayakawa, S., Masai, K., & Hughes, J. P. 1988, PASJ, 40, 639
Ponman, T. J., Bertram, D., Church, M. J., Eyles, C. J., Watt, M. P., Skinner, G. K., & Willmore, A. P. 1990, Nature, 347, 450
Raymond, J. C., & Smith, B. W. 1977, ApJS, 35, 419
Rephaeli, Y. 1978, ApJ, 225, 335
Salem, S. I., Panossian, S. L., & Krause, R. A. 1974, Atomic Data Nuclear Data, 14, 91
Turner, M. J. L., et al. 1989, PASJ, 41, 345
Warwick, R. S., & Stewart, G. C. 1989, in Proc. 23d ESLAB Symp. on Two Topics in X-Ray Astronomy, ESA SP-296, Vol. 2, 727
Watt, M. P., Ponman, T. J., Bertram, D., Eyles, C. J., Skinner, G. K., & Willmore, A. P. 1991, preprint
Zabludoff, A. I., Huchra, J. P., & Geller, M. J. 1990, ApJS, 74, 1